Available online at www.CivileJournal.org

Civil Engineering Journal

(E-ISSN: 2476-3055; ISSN: 2676-6957)

Vol. 9, No. 09, September, 2023

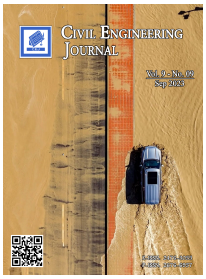

Subsurface Analysis Using Microtremor and Resistivity to Determine Soil Vulnerability and Discovery of New Local Fault

Adi Susilo [1, 2], Alamsyah M. Juwono [1*], Faridha Aprilia [1, 2], Farizky Hisyam [1], Siti Rohmah [1], Muhammad Fathur Rouf Hasan [1, 3]

[1] *Department of Physics, Universitas Brawijaya, Malang, 65145, Indonesia.*

[2] *Research Centre of Geosience and Hazard Mitigation, Universitas Brawijaya, Malang, 65145, Indonesia.*

[3] *Department of Civil Engineering, Politeknik Negeri Jakarta, Depok, 16425, Indonesia.*

Received 29 April 2023; Revised 14 August 2023; Accepted 17 August 2023; Published 01 September 2023

Abstract

Microtremor and geoelectrical resistivity surveys have been conducted in areas where the April 10, 2021, earthquake of 6.1 Mw caused the most damage. Wirotaman Village, Malang Regency, was one of the regions with the most extensive damage. This study aims to investigate the seismic vulnerability and subsurface conditions that result in severe damage at the research location. This study's Horizontal to Vertical Spectral Ratio Analysis (HVSR) curve was derived from the recorded microtremor signal in the frequency domain. The frequency parameter and amplification factor obtained from the curve are used to determine the seismic vulnerability index. In addition, a geoelectrical resistivity study with a dipole-dipole configuration was conducted at the site with the most extensive damage. The results of this study show the correlation between the results of the HVSR curve analysis and geoelectrical resistivity in determining the seismic vulnerability of an area. The results indicated that the high seismic vulnerability index value ranged from K_g = 12.0 to 18.0, with the most severe damage concentrated in the Southwest at SA 05 and SA 06. Based on the results of the geoelectrical survey, information was obtained that several points of damage to buildings at SA 05 (red circle) were on the same line, where this condition was associated with the possibility of new faults at that location. This microtremor and geoelectric resistivity investigation reveals thick sedimentary deposits with a high seismic vulnerability index and low resistivity. This study's findings can be utilized as a guide for micro zonation studies in research areas. This research contributes to the surrounding community in the form of disaster mitigation, where construction must avoid local fault positions that have been found to reduce the level of damage when natural geological disasters occur.

Keywords: Microtremor; Seismic Vulnerability; Geoelectrical Resistivity; Earthquake Disasters; Soil.

1. Introduction

Malang Regency, in the eastern part of Java, has a high frequency of earthquake disasters. According to the Malang Regency Regional Disaster Management Agency's (BPBD) disaster inventory statistics, 76 earthquakes in the Malang Regency area occurred between 2019 and 2021 [1]. The April 10, 2021, earthquake with a magnitude of 6.1 Mw caused significant destruction in the Malang area. The earthquake's epicenter was 96 kilometers southwest of Malang and 80 kilometers deep [2]. Wirotaman Village, Ampegalding District, Malang Regency, is one of the sites where the earthquake caused significant damage. According to the Malang Regency BPBD report, the April 10, 2021, earthquake

* Corresponding author: amjuwono@ub.ac.id

http://dx.doi.org/10.28991/CEJ-2023-09-09-014

resulted in 66 injuries, four fatalities, 786 displaced persons, 5,750 houses with minor damage, 3,894 houses with moderate damage, and 1,716 houses with severe damage [1]. Considering the location of Ampelgading District, which is relatively distant from the earthquake's epicenter, it is suspected that there are local effects, one of which is the local lithology and geological structure, which are capable of causing quite significant earthquake tremors.

The geophysical survey is the most crucial technique for determining the subsurface structure, one of which is the microtremor survey, commonly used as an initial approach. This survey is conducted to determine the ground's resistance to the effects of seismic vibrations. Microtremor is a continuous ground vibration with a small magnitude induced by both natural and human activity and dependent on the local geological conditions [3]. Horizontal-to-Vertical Spectral Ratio (HVSR), commonly referred to as H/V or the Nakamura approach, was utilized to examine microtremor signals [4]. According to Nakamura, the primary frequency and peak value of HVSR (also referred to as the soil amplification factor) are connected to the H/V ratio component of microtremor recordings [5].

Several studies have used the HVSR approach to determine the risk of earthquakes. Lermo & Chávez-García (1994) examined the areas of Mexico City that were repeatedly devastated by the great earthquakes of 1957, 1979, and 1985 [6]. Several other studies have used the HVSR method to evaluate several cities with a high risk of earthquake disasters, such as Jammu Barat and Vishakhapatnam, India [7, 8], Bandar Lampung and Jakarta, Indonesia [9, 10], and Ivanec, Croatia [11, 12]. The HVSR method was also used to evaluate local effects when the Ezgeleh earthquake occurred on November 12, 2017 with a magnitude of 7.3 [13], the Albania earthquake on November 26, 2019 with a magnitude of 6.4 [14], the Changning earthquake in 2019 [15], and the Izmir, Turkey, earthquake on October 30, 2020 [16].

In subsequent studies, the geoelectric resistivity method was utilized to assess the structure of faults in regions with high seismic hazard levels. The geoelectric method operates by injecting an electric current into the subsurface using two electrodes to determine the subsurface resistivity [17]. The resistivity cross-section can be used to identify rock layers and the direction of the subsurface structure [18]. Many additional geoelectrical resistivity studies have been conducted to prevent geological disasters, such as identifying structures (faults) and subterranean lithology that can trigger geological disasters [19–21].

Many academics have conducted numerous studies on earthquake potential in the Malang Regency area [22, 23]. Peak Ground Acceleration (PGA) modeling conducted by Chasanah et al. (2022) showed that with a PGA value of 23.687–33.069 gal, it would produce damage equivalent to the IV-V MMI scale [22]. This level of damage is capable of triggering the appearance of ground cracks. Muntafi & Nojima (2021) conducted microzonation in the Malang Regency area after the April 10, 2021, earthquake, resulting in the South Malang spectral acceleration value being higher than other regions [23]. These studies show that the micro zonation efforts that have been carried out have not used HVSR analysis. Regional HVSR analysis has been carried out by Tawakal et al. (2020) to determine the value of the shear wave velocity (Vs30) in East Java. The analysis results show that the southern region of East Java (including Malang Regency) is dominated by medium- to hard-rock soils [24]. However, this HVSR analysis has not yet been used for micro zoning earthquake risk assessment. The analysis results also do not provide a detailed description of the lithology and subsurface structure. This can be corrected by correlating the HVSR and the geoelectrical resistivity analysis. Among others, Keskinsezer & Dağ (2019) [25], Khalili & Mirzakurdeh (2019) [26], and Demirci et al. (2007) [27] have researched combining microtremor and geoelectric resistivity data analysis to assess subsurface conditions.

This study utilized microtremor analysis results to establish which parts of Wirotaman Village are most vulnerable to earthquakes. It is believed that areas with the highest level of seismic sensitivity are connected with thick sediment deposits and geological features. The value of the dominant frequency and seismic vulnerability index derived from the HVSR curve analysis of microtremor signals determines the soil classification and level of vulnerability [3]. Follow-up measurements with the geoelectrical resistivity method can reveal thickness, lithology, and subsurface structure information. This study attempts to determine the seismic vulnerability of Wirotaman Village based on the seismic vulnerability index derived from the processing of microtremor recordings' HVSR curves. Based on resistivity measurements, this study also examined subsurface conditions in the areas of Wirotaman Village most damaged by the April 10, 2021 earthquake. Therefore, this research aims to analyze the seismic vulnerability in Wirotaman Village and the lithology and subsurface structures based on the analysis of the HVSR curve and geoelectric resistivity. As part of earthquake mitigation, this effort aims to investigate micro zonation in the research area.

2. Methodology

2.1. Research Methodology

Generally, the flow of research begins with a literature review based on previous research and data or information on disaster events at the research location. The research location survey aims to conduct a preliminary study related to field conditions directly to prepare the survey design. The research design was arranged at the same location for the microtremor and resistivity geoelectric methods. This is done so that the results of the two methods can be compared. The research flow is shown in Figure 1 below.

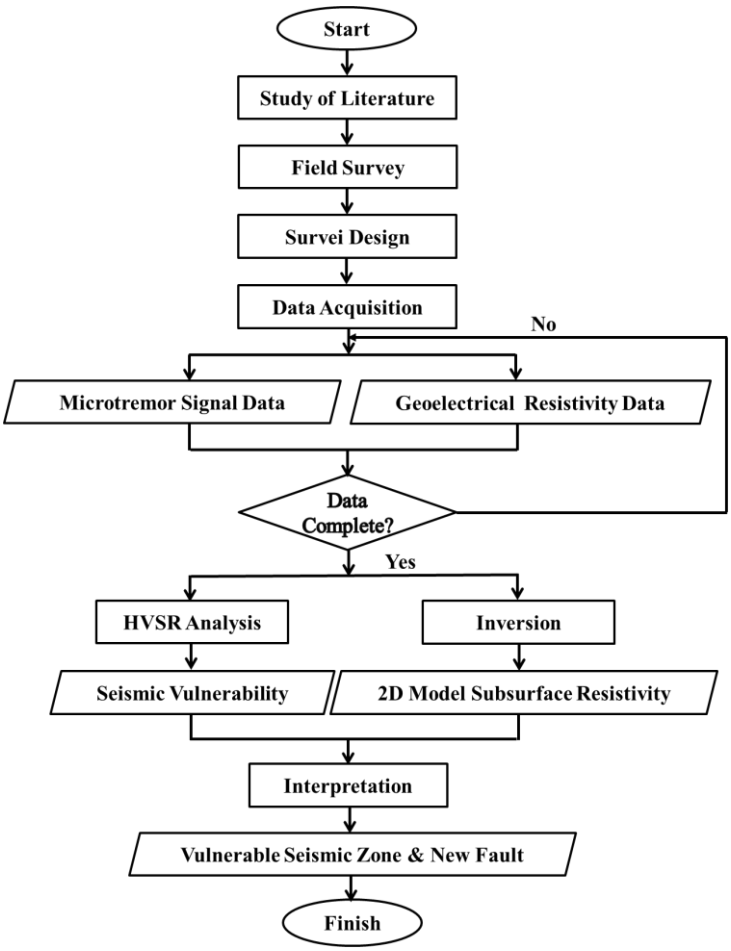

Figure 1. Flowchart of research

Research employing the microtremor technique was conducted at six measurement stations spanning 1 square kilometer (Figure 2). The distance between measurement points ranges from 200 to 500 meters. In addition, the geoelectrical resistivity method was conducted at site SA 05 along two points of 10 meters and 100 meters in length, with a 10-meter spacing between electrodes. The selection of Point SA 05 for geoelectrical resistivity measurements was influenced by the fact that the April 10, 2021, earthquake caused the most damage in this region.

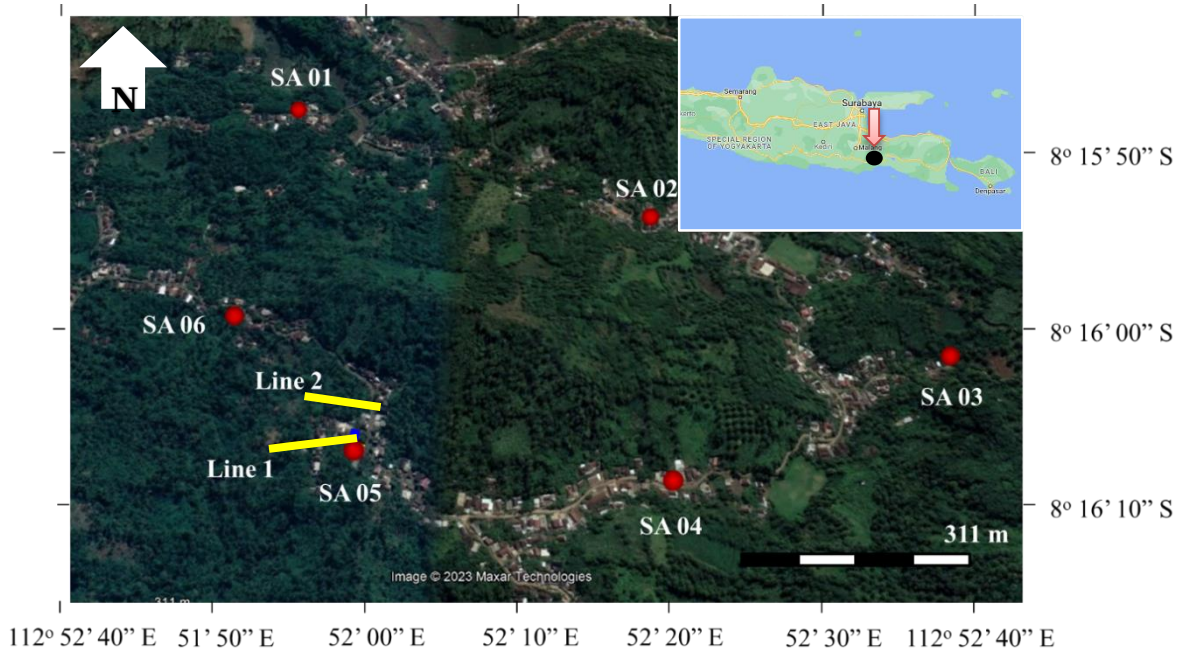

Figure 2. The research design for microtremor (red dot) and Geoelectrical resistivity (yellow line) measurements in Sukoanyar Hamlet, Wirotaman Village, Ampelgading District, based on Google Earth imagery

2.2. Microtremor Method

The microtremor signal was recorded using the Digital Portable Seismograph TDL-303S. Taking into account the noise, microtremor measurements were conducted with a sample rate of 100 Hz for 30-45 minutes at each measurement point. Signals at measurement points that have much noise are recorded for an extended period. This is done to obtain suitable signals for analysis based on the criteria of the SESAME (Site Effects Assessment using Ambient Excitation) project. SESAME (Site Effects Assessment Using Ambient Excitation) raises the issue of local effects in earthquake risk mitigation efforts, particularly in urban areas. According to SESAME, the minimum recording time for a signal with a dominant frequency between 0.2 and 10 Hz is between 30 and 2 minutes. The shorter the recording period required, the higher the expected signal frequency.

The acquired data is a three-component microtremor signal (North-South, East-West, and Up-Down) in the temporal domain. A Butterworth band pass filter is applied to the data. The minimum frequency restriction is set at 0.5 Hz, and the maximum frequency limit is set at 25.0 Hz. This frequency limit's separation depends on the frequency values of microtremor signals [28]. The filtered signal is separated into several windows whose widths are determined by the SESAME European criteria. The signal's duration must meet these conditions: the number of windows multiplied by the window width. For instance, if the anticipated microtremor frequency is 2 Hz, the minimum recording time advised is 5 minutes [29]. Using an anti-triggering logarithm, the Short Term Average (STA) and Long Term Average (LTA) can be compared to determine the window automatically. STA refers to the average short-term signal amplitude (0.5–2.0 s), whereas LTA refers to the average long-term signal amplitude (>10.0 s). In this analysis, the STA is 1.00 seconds, whereas the LTA is 30.00 seconds. The signal is considered a microtremor if the STA/LTA ratio exceeds the required threshold, defined as 0.20 s minimum and 2.50 s maximum [29].

In the subsequent stage, HVSR analysis is performed by comparing the Fourier spectrum of the signal's horizontal component A_H to that of the vertical component A_V:

$$\frac{H}{V} = \frac{A_H}{A_V} = \frac{\sqrt{\left(A_{(N-S)}(f)\right)^2 + \left(A_{(E-W)}(f)\right)^2}}{A_{(V)}(f)} \quad (1)$$

where $A_{(N-S)}(f)$ and $A_{(E-W)}(f)$ are the Fourier spectra of the horizontal and $A_{(v)}(f)$ is the vertical signal. This comparison will generate an HVSR curve with the frequency on the ordinate axis and the HVSR on the abscissa axis. The Geopsy software is utilized for the microtremor signal processing stage.

The validity of the HVSR curve can be determined through testing against several parameters. Initially, the number of essential cycles must exceed 200. We then multiply the window width by the number of windows obtained and the HVSR peak frequency to determine the number of essential cycles. Second, the HVSR curve's peak frequency (f_0) must be more than ten divided by the window width [29]. The dominant frequency and amplification factor can be used to calculate a seismic vulnerability index that describes the risk of earthquake-related damage caused by soil variables. The seismic vulnerability index (K_g) is calculated using the following formula:

$$K_g = \frac{(A_g)^2}{f_o} \quad (2)$$

where f_o and A_g are the dominant frequencies and soil amplification factors derived from HVSR analysis [30].

2.3. Geoelectrical Resistivity Method

The geoelectrical resistivity method is an active geophysical method that injects current into the Earth through a pair of current electrodes, C1 and C2. The response is produced as a difference in potential between two electrodes, P1 and P2. The tool utilized to collect data for this study is a resistivity meter. The geoelectrical resistivity method attempts to identify the subsurface conditions with the highest seismic vulnerability value at the research location. This study used a dipole-dipole configuration since it is beneficial for mapping. This configuration is considered sensitive for detecting vertical discontinuities [25]. The distance between potential and current is in the dipole-dipole configuration. In addition, the distance between the current and potential electrodes increases to na, where n is an integer (Figure 3) [31].

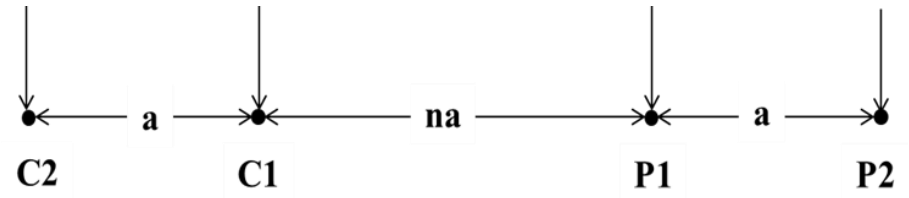

Figure 3. Current and potential electrode circuits in a dipole-dipole configuration

The geometric factor k of the dipole-dipole configuration is expressed in the equation:

$$k = \pi n(n+1)(n+2) \quad (3)$$

Based on the geometric factor value, the apparent resistivity value can be determined through the equation:

$$\rho_a = k\frac{\Delta V}{I} \quad (4)$$

where ρ_a is the apparent resistivity, ΔV is the potential difference measured by the potential electrode, and I is the value of the injected current. This apparent resistivity value was inverted with RES2DInv software to obtain a 2D section of the subsurface resistivity value.

3. Result and Discussion

3.1. Geological Conditions of the Study Area

As a result of subduction between the Indo-Australian and Eurasian plates, the study area is tectonically part of the Sunda arc series. The active Quaternary volcanoes such as Mount Semeru, Mount Bromo, and Mount Arjuna are north of the research location. The Southern Mountains, part of the Miocene "Old Andesite" volcano, are in the South [32]. The research site's topography consists of hills, notably Mount Manggisan in the Southwest and Mount Bagong in the North. Southwest and southward flows the Turanggondo River, while the Manggis River flows northeastward.

Based on Figure 4 of the geological map of the Turen sheet [33], the lithology of the study area consists of the Middle Miocene-aged Wuni Formation (Tmw), which is formed of basalt andesitic breccia and lava, tuff breccia, breccia lava, and sandy tuff. The older Mandalika Formation (Tomm) is located in the southeastern portion of the study area. It dates back to the Late Oligocene to the early Middle Miocene. Mandalika Formation consists of andesite lava, basalt, trachyte, dacite, and pyrophilitic andesite breccias. The contact between the two formations is exposed on the surface of the research area as a southwest-northeast oriented Pointament, which is suspected as a fault. This structure is a normal fault structure assumed to have evolved in the Late Tertiary (Plio-Pleistocene), while the Wuni formation is unconformity "overlapping" the Mandalika Formation.

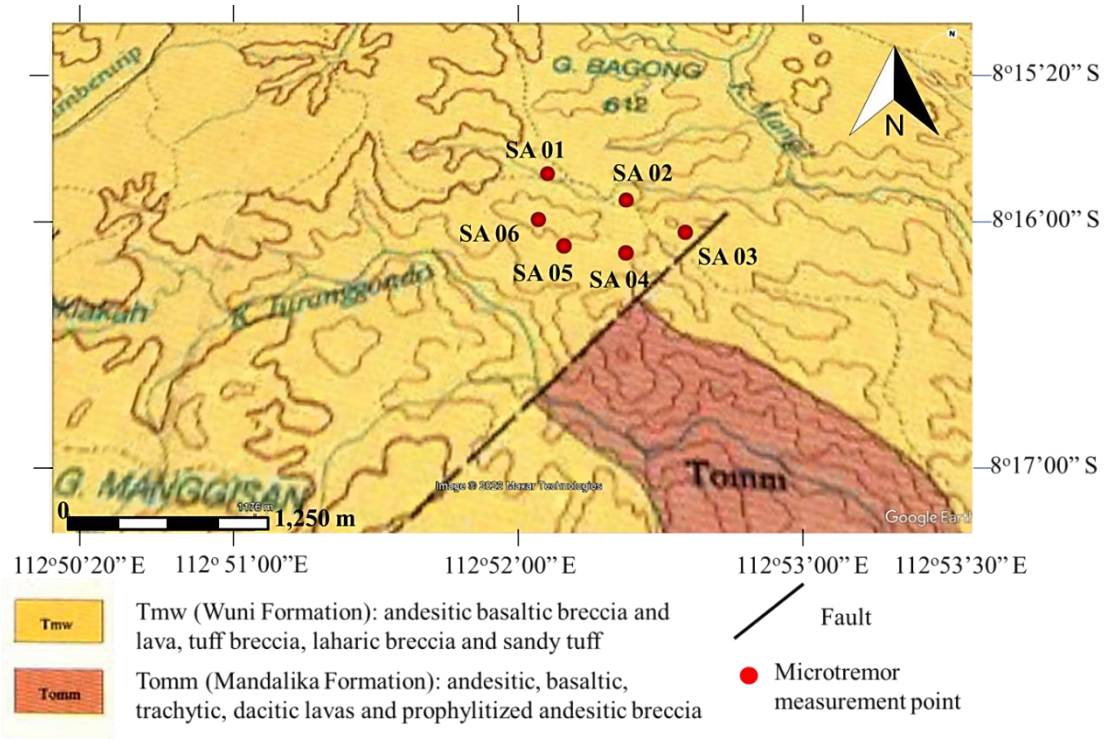

Figure 4. Geological map of the study area (modified by Sujanto et al., 1992 [33])

According to the preliminary field survey, the research site's surface layer consists primarily of clay to sandy loam. The research area consists of hilly slopes that range from gentle to steep. A fracture in the local hamlet hall's floor was discovered approximately 10 meters to the North of Point SA 05 (Figure 5). In addition to a crack in the floor of the local hamlet hall, there was a spring streaming from a slope around 200 meters North of Point SA 05.

(a) (b)

Figure 5. (a) Demolished homes surround the state of hamlet hall. The structure that collapsed due to the earthquake on April 10, 2021, has not yet been reconstructed (June 2022). (b) Cracks occurred on the hamlet hall floor due to the April 10, 2021 earthquake.

3.2. HVSR Curve

The resulting microtremor recording is in the form of a time-domain signal. In addition, the data for the three-component signal are evaluated using the Fast Fourier Transform (FFT) technique. The frequency domain HVSR curve is the outcome of the transformation. The HVSR curve is the outcome of processing the microtremor data, as seen in Figure 6. The curve has an abscissa in the form of a frequency value and an ordinate in the form of a H/V value. In addition, the figure contains the standard deviation value and the mean HVSR curve.

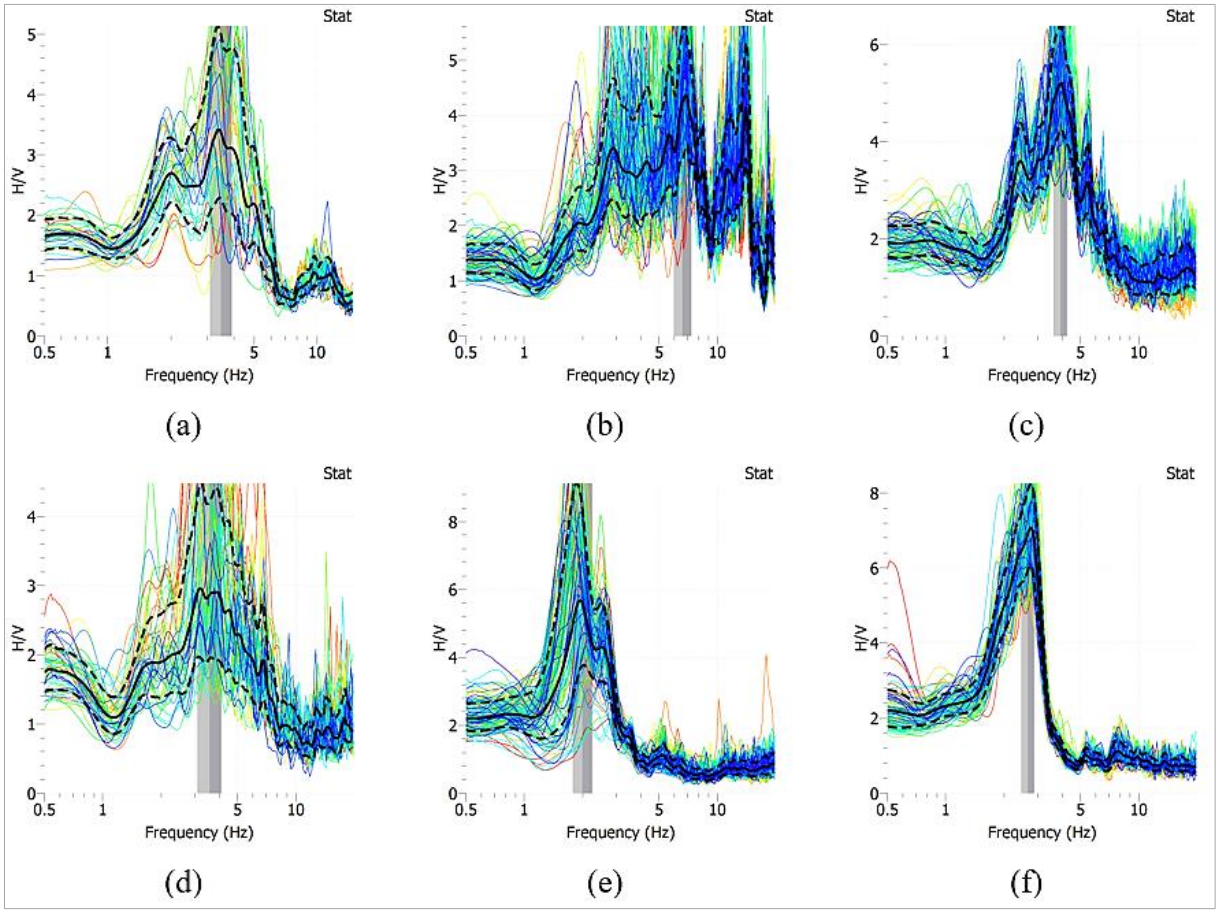

Figure 6. HVSR curve at point (a) SA 01 (b) SA 02 (c) SA 03 (d) SA 04 (e) SA 05 (f) SA 06. The thick black point shows the average HVSR value based on FFT analysis. The curve also displays the standard deviation of the HVSR curve in the dotted black point.

There are numerous variants in the HVSR curve's peak pattern. Following the HVSR curve depicted in Figure 6, points SA 01, SA 03, SA 04, SA 05, and SA 06 exhibit a pattern with a single peak. However, only SA 05 and SA 06 feature single peaks that are quite distinct. In the meantime, the HVSR analysis results at site SA 02 exhibit a single, unclear peak curve. Young Quaternary sedimentary material exhibits a microtremor signal response, as the curve shows a highly distinct single peak. In contrast, an HVSR curve with indistinct or even flat peaks suggests the existence of hard rock beneath the surface [34]. Consequently, sedimentary material dominates the lithology at SA 05 and SA 06, whereas hard rock dominates at SA 02.

Subsurface geological conditions and the microtremor data recording process cause the difference in the shape of the HVSR curve in each measurement. The characteristics of the HVSR curve are shown by the curve pattern formed; this curve pattern is used for local geological characterization. Several parameters that affect the pattern of the curve are the value of the frequency dominant factor (f_0) and the soil amplification value (A_0) generated at each measurement point. The topology of the HVSR curve in the study area includes the HVSR curve with one peak and the HVSR curve with a wide peak.

The shape of the curve with one clear peak is found in the HVSR curve, appearing as one single peak with a significant value. One of the microtremor measurements in the study area is indicated by point SA 06. The single peak on the resulting curve indicates an impedance contrast at a certain depth so that the wave experiences amplification or reinforcement. The curves with broad peaks are shown at points SA 01, SA 04, and SA 05. The HVSR curve with a wide peak may be related to local geology or geometry related to a sloping bedrock basin; it can also be due to variations in the sedimentary structure of the bedrock.

3.3. Dominant Frequency

The dominant frequency value of the HVSR curve at each measurement point is plotted on the map. Then, interpolation is conducted using the Kriging method to obtain a dominant frequency map. The contour Points on the map indicate the main frequency values in the research area. The dominant frequency value is the frequency value at the peak of the HVSR curve. Figure 7 depicts the results of the dominating frequency distribution map in the study area.

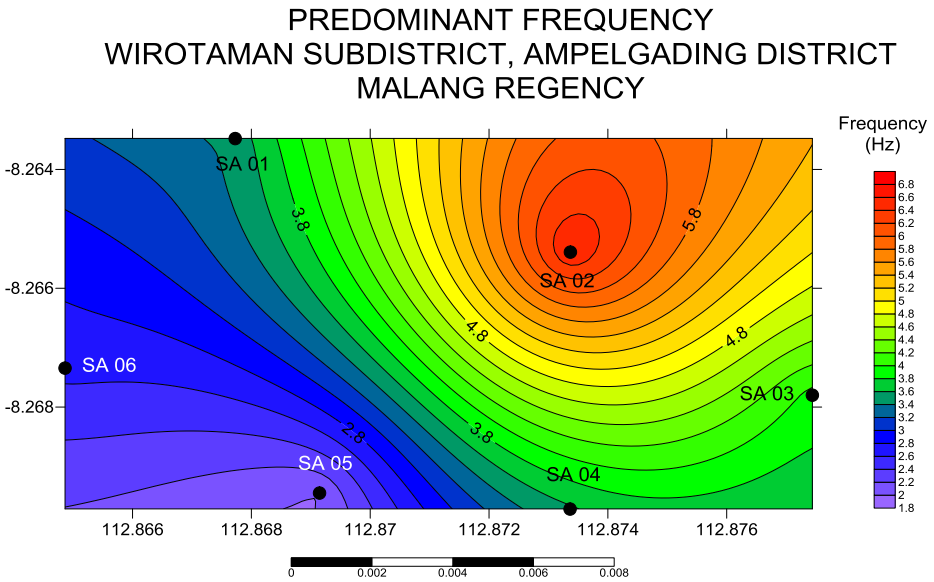

Figure 7. Map of dominant frequencies in the research area

According to Figure 7, the dominating frequency value at the research site spans from 2.0 Hz to 6.8 Hz. According to Kanai [3] soil classification, the soil types in the research region range from class I to class III. Class III rocks' distribution is located at point SA 05 in the northeast of the study area. Then, in an increasingly southwesterly direction, it shifts to class I. According to Kanai [3], class I soils consist of Tertiary sandstones and coarse gravel. Class III soil, meanwhile, is typically composed of alluvial silt and is characterized by its extreme softness. This suggests that the sediment layers in the studied area become heavier as one move southwestward. According to the Omote-Nakajima soil classification [3], a dominant period of 0.15 to 0.50 seconds indicates that the soil type ranges from type A to type C. Places with soil type C have a soft topsoil layer that extends to a depth of at least 30 meters.

Based on Figure 7, the dominant frequency value of the soil (f_0) at the study site ranges from 2.0 Hz to 6.8 Hz. Based on soil classification [3], soil types in the study area are included in class I, III, and IV. Class I soil classification is found at point SA 05 with a dominant frequency value (f_0) <2.5 Hz; this area is described as having a very thick layer of

sediment, consisting of alluvial rock formed from deltaic sedimentation, while the top soil layer (topsoil) consists of mud with a depth of ± 30 m. Class III rocks are distributed at points SA 01, SA 03, SA 04, and SA 06, which are located in the northeast of the study area. Soil classification in that area has a dominant frequency value (f_0) between 2.5 Hz to 4 Hz. This area is described as having sedimentary layers in the thick category (±10-30 m) consisting of gravelly sand, hard clay, clay, and loam types. Then to the southwest, it shifts to class IV; this area is at point SA 02 with the dominant frequency value (f_0) 4 Hz – 10 Hz. This area is described as having a moderate thickness of sediment layers between 5-10 m with almost the same constituent rocks as type III. According to the Omote-Nakajima soil classification [3], a dominant period of 0.15 to 0.50 seconds indicates that the soil type ranges from type A to type C. Places with soil type C have a layer of soft humus that extends to a depth of at least 30 meters.

The dominant frequency relates to the dominant period of the soil. The dominant period value of the land in a place is inversely proportional to the dominant frequency value. Domianna frequency value (f_0) is used to estimate the thickness of the surface layer in the area studied. While the value of the dominant period (T_0) is used to estimate the level of rock hardness. Areas with low dominant frequency values will be vulnerable to vibrations with long periods that can threaten buildings.

3.4. Amplification Factor

The HVSR curve analysis can also determine the value of the amplification factor at the measurement point, in addition to the dominating frequency parameter. The amplification factor is determined by examining the HVSR curve's maximum value. The amplification factor is the ratio of the free surface ground vibrations to the bedrock ground vibrations [35, 36]. Thus, the amplification factor can provide an overview of the local consequences of an earthquake [11]. This amplification factor is determined by determining the HVSR curve's peak value. Figure 8 depicts a map showing the distribution of amplification factor values in the research area.

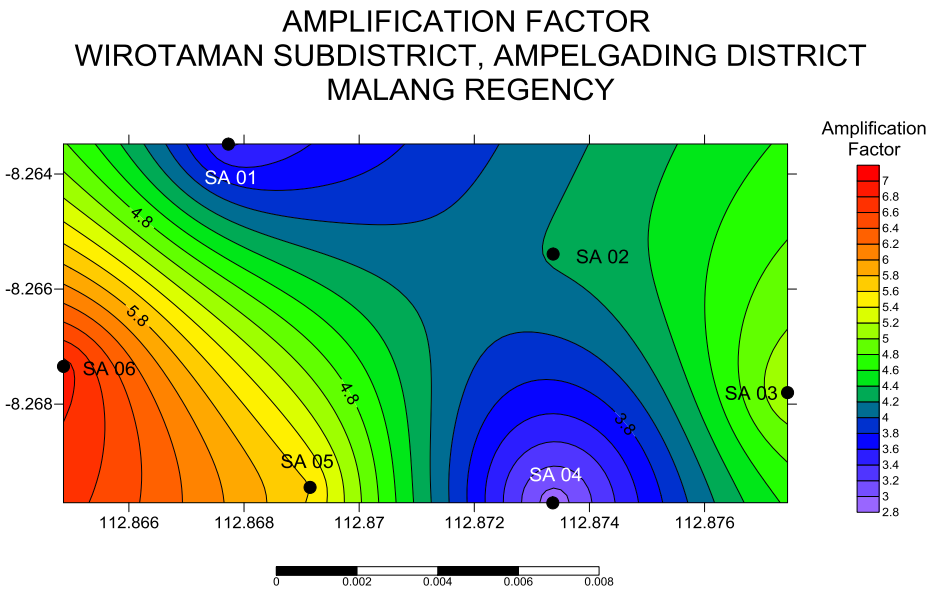

Figure 8. Map of dominant frequencies in the research area

According to the map of the amplification factor, the value of the amplification factor generally increases from east to west. The amplification factor is the highest at Point SA 06 (A=6.89), whereas Point SA 02 (A=2.86) is the lowest. This indicates that when an earthquake happens at Point SA 06, the infrastructure will suffer vibrations that are 6.89 times stronger than those of the bedrock. A high amplification value implies an impedance contrast near the surface, namely soft sediment deposits on the surface and loose material on slopes prone to landslides.

According to Nakamura (2000), amplification can occur due to the magnification of seismic waves caused by striking differences between layers [37]. This can be interpreted as seismic waves enlarging if they pass through a soft medium to a hard medium. If the difference is greater, then the wave magnification is also greater. So it can be concluded that the soil amplification value (A_0) is related to the soil sediment layer. If the soil amplification value (A_0) is large, the sediment in that area is getting softer; conversely, if the soil amplification value (A_0) is low, the sediment layer is getting harder.

3.5. Seismic Vulnerability Index

The seismic vulnerability index is a measurement that summarizes a region's vulnerability to earthquakes. The seismic vulnerability index quantifies the soil or ground surface's vulnerability to displacement during an earthquake [38]. Figure 9 depicts the distribution map of seismic vulnerability index values in the study area.

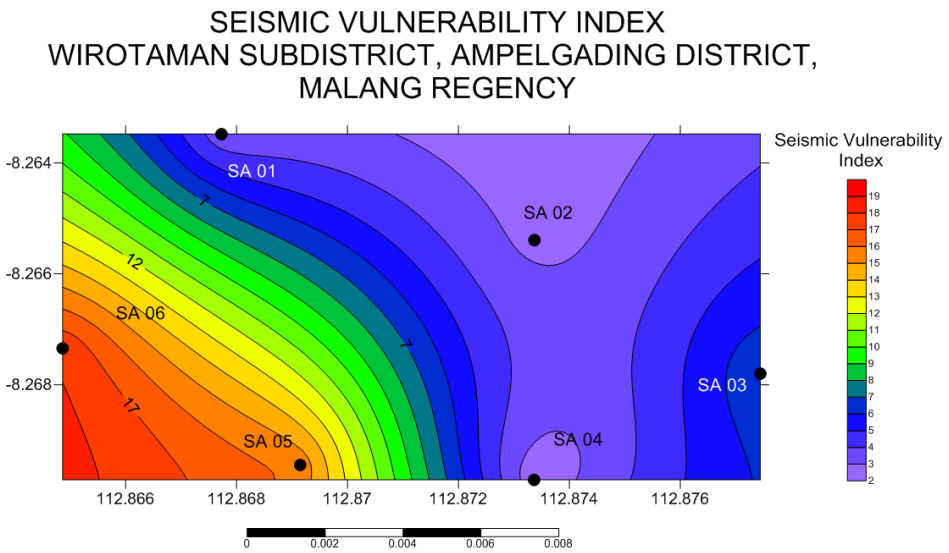

Figure 9. Seismic vulnerability map of the study area

The seismic vulnerability value describes the sensitive zone. When an earthquake strikes, high seismic vulnerability values indicate a significant danger of damage. In the study area, the seismic vulnerability index ranges from the lowest (K_g=2.284) at point SA 02 to the maximum (K_g=17.836) at point SA 06. Points SA 05 and SA 06, which are the most vulnerable, have a high seismic vulnerability index value between K_g=12 and 18, which corresponds to a high seismic vulnerability index value between K_g=12 and 18. In contrast, the areas surrounding SA 01, SA 02, SA 03, and SA 05 tend to be relatively earthquake-safe due to their low seismic vulnerability index.

The seismic vulnerability index value (Kg) is used to estimate an area that is prone to ground motion based on the relationship between the soil dominant frequency value (f_0) and the soil amplification value (A_0). The seismic vulnerability index (Kg) ranged from 2.284 to 17.836 in the study area. The low seismic vulnerability index value is at point SA 02 (Kg=2.284), while the high seismic vulnerability index value is at point SA 06 (Kg=17.836). The points SA 01, SA 02, SA 03, and SA 05 have seismic vulnerability index values ranging from 4 to 15. High seismic vulnerability index (Kg) values are obtained in areas with high amplification and low dominant frequency values. This result is related to the condition of the thick sediment layer with high compactness making it vulnerable to vibration. Vice versa, low seismic vulnerability index values are obtained in areas with low amplification values and high dominant frequency values. This result is related to the condition of a thin layer of sediment with a low impedance contrast so that it is quite strong against vibrations; this area is generally located in a hilly area.

3.6. Geoelectrical Resistivity

The SA 05 and SA 06 points are located at the locations with the biggest seismic vulnerability index values, as determined by the seismic vulnerability index analysis. However, only geoelectrical resistivity measurements were conducted at Point SA 05, based on field observations of the extent of building damage and visual observations of cracks in the building's floor. Geoelectrical measurements were carried out in two Points separated by 60 meters. Point 1 has a length of 150 meters with an East-West orientation. This path is to the south of the hamlet hall fracture. Four iterations of the inversion process produced a model as a 2D resistivity cross-section of Point 1, as depicted in Figure 10.

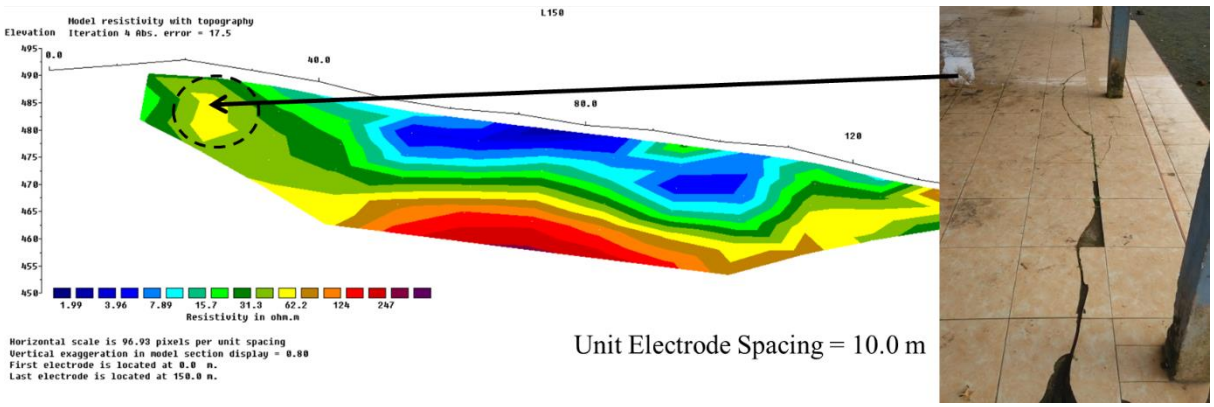

Figure 10. A cross-section of the resistivity of Point 1 and the fracture on the floor of the hamlet hall appears on the sandy clay lithology

According to Figure 10, the resistivity value of the rocks along Point 1 ranges from 1.99-247 Ωm with a maximum depth of 25 meters. The interpretation phase entails comparing the resistivity values derived from the inversion modeling to a table of rock resistivity values, local geological conditions, and the findings of visual field observations. The interpretation achieved a very low resistivity value of 1.99–7.89 Ωm with a color range from light blue to dark blue. This extremely low resistivity value dominates the surface of Point 1, particularly between 40 and 120 meters from the east end of Point 1. The very low resistivity lithology is 10 to 20 meters thick at that point. Its lithology is considered a clay layer due to its extremely low resistivity value. Medium resistivity values (7.90–62.22 Ωm) are indicated by light green, yellow, and orange. This medium-resistivity lithology is interpreted as a layer of sandy clay. At a depth of 15 to 20 meters below the surface, a lithology with a high resistivity value (reddish-purple color) and a resistivity range of 62.3-246 Ωm is discovered. According to the resistivity characteristics, this is likely bedrock. The high resistivity lithology is related to the strata of volcanic breccia that make up the Wuni Formation. As compared to field data, the fracture that occurred at Hamlet Hall after the April 10, 2021, earthquake correlates to a lithological discontinuity of sandy clay.

Figure 11 shows point 2 is 100 meters long and oriented east-west. Four repetitions of the inversion procedure were performed to create the inversion model depicted in Figure 11 for Point 2. According to the Point 2 inversion modeling results, the range of rock resistivity values is between 1.99 and 246 Ωm. Furthermore, this resistivity value is divided into three layers, namely layers with low resistivity values, 1.99-7.89 Ωm (dark blue-light blue); medium resistivity, 7.90-62.1 Ωm (light green-orange), and high resistivity, 62.2-246 Ωm (red-dark red). In Point 2, rocks with low resistivity are dispersed 10 to 20 meters below the surface. The low resistivity value on Point 2 is interpreted as an aquifer-like breccia layer. This aquifer appears to break through to the surface vertically until it finally appears as a spring. This spring is located around 5 meters to the North of Point 2. This spring's presence indicates a weak zone, which is regarded as a fracture. In addition, moderate resistivity values are distributed around the surface of Point 2. These intermediate resistivity values are regarded as sand-clay and humus layers. At a depth of 20 meters below the surface, significant resistivity readings are identified as a layer of volcanic breccia inside the Wuni Formation.

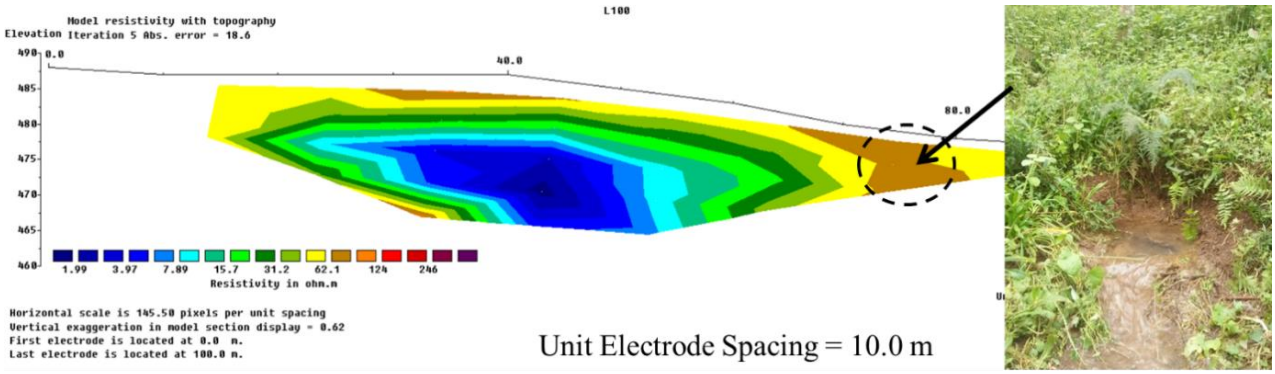

Figure 11. Subsurface resistivity section at Point 2. The appearance of a spring at a point 5 meters north of Point 2 is related to a layer of sandy clay

3.7. Discussion

It is anticipated that the combination of information on the seismic vulnerability index values and geoelectric data on top-of-the-earth satellite imagery will provide an overview of the subsurface conditions that triggered the April 10, 2021, earthquake that caused extensive damage in Wirotaman Village. The findings of overlaying the seismic vulnerability index map on satellite imagery in the study region (Figure 12) reveal high seismic vulnerability values in the southwest of the study area, namely in the vicinity of Points SA 05 and SA 06. Points SA 05 and SA 06, which have a high seismic vulnerability index value, are the most vulnerability to ground vibrations, notably those caused by earthquakes. These two Points sustained the most severe ground damage when the earthquake struck on April 10, 2021. This demonstrates that the region with the highest seismic vulnerability is a weak zone that will sustain substantial damage in an earthquake [39].

Moreover, the high seismic sensitivity values at SA 05 and SA 06 match the low dominant frequency values and the high amplification factors. This shows that thick sediments exist to the southwest of the research site. The sediment is formed of loosely degraded Tertiary volcanic debris and is relatively thick in the southwest portion of the research site. Following the concept of the site effect, rock materials combined with thick sediments will amplify the effects of earthquake shocks. Intriguingly, the severely damaged houses at Point SA 05 are aligned north to south across the hamlet hall, as determined by direct field observations. The SA 05 measurement point is approximately 50 meters east of the hamlet hall. If a straight point is made from Point SA 05 to Point SA 06, the houses with the most severe damage face southeast-southwest. In actuality, there is a collapsed mosque near the location of Point SA 06 owing to the earthquake.

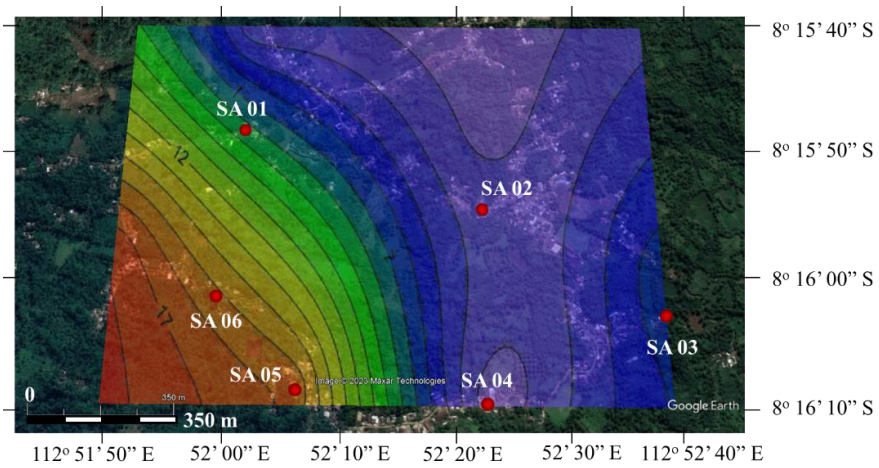

Figure 12. The results of the seismic vulnerability index map overlay at the measurement location

Moreover, to establish the thickness of the sediment layer that creates a high seismic vulnerability index in the southwest of the research area, particularly around Point SA 05, two Points of geoelectric resistivity measurements were conducted over the dipole-dipole configuration. Sedimentary material with low resistivity dominates the area surrounding Point SA 05, which has a high seismic vulnerability index value, as shown in Figure 13. To the west of the route, the clay and sandy loam sediment layers are increasing in thickness. This suggests a thickening of sediments to the southwest of the study site. The area surrounding Points SA 05 and SA 06 on the geological map lies on the slopes of the hills bordering the Turanggondo River. This element enables the accumulation of alluvial material and slope erosion, resulting in a thick sediment layer in the study's southwest area.

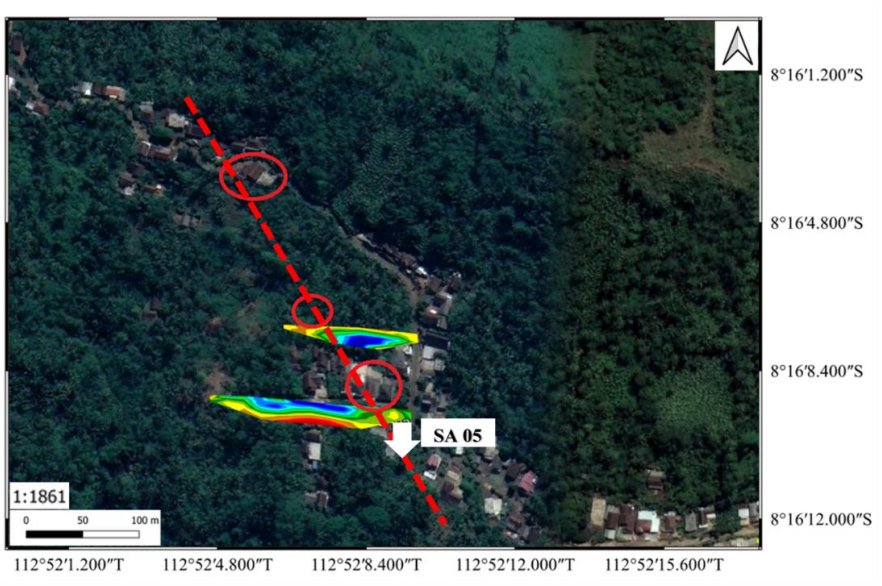

Figure 13. The results of the resistivity cross-section overlay on Point 1 and Point 2 at the measurement location

Figure 13 shows three red circles, with the bottom and top circles representing the settlements that sustained the most severe harm while the surrounding settlements were unaffected. In addition, in the circle in the center, a spring appears on the ground; this spring indicates the presence of a weak zone, interpreted as a fracture. If a straight line is drawn, the three circles are in one line; this condition is associated with the possibility of a new fault at that location. The emergence of new faults may occur, considering that the location of SA 05 is quite close to the fault that separates the Wuni and Mandalika formations (Figure 4), which is about 750 meters, so it is only natural that the damage to buildings caused is also quite severe.

The houses that were destroyed around points SA 05 and SA 06 have been reconstructed; some are still left damaged and some are occupying temporary housing. In the sector of infrastructure, the building frequency value may differ from the dominant frequency of the land while constructing buildings in the area. This can cause resonance events, increasing the shaking of buildings during an earthquake [12]. This must be considered because the research area is tectonically active and has the potential for future big earthquakes. In addition to the earthquake risk, a crack traversing the hamlet

hall (bottom red circle in Figure 13) and the formation of springs near SA 05 also require consideration. This is because the existence of soil fissures and springs could indicate the presence of ground motion. Other hazards, such as landslides, can be triggered by topographic characteristics that tend to be slope-shaped when heavy rainfall or earthquakes occur. Surveys of S-wave velocity in the study area and probe data make it possible to acquire a more precise soft layer thickness. As suggested by the appearance of fissures following the April 10, 2021 earthquake, additional geophysical investigations can demonstrate the existence of a subsurface geological structure.

Based on the microtremor survey, it was found that areas showing indications of faults had a low dominant frequency (f_0) value (<2.5 Hz), while the results of the geoelectrical resistivity survey showed a resistivity value of 62.2 Ω (clay). The clay layer has a low resistivity value due to the negative ions' content and the membrane polarization process. Based on the research of Rochman et al. (2023) conducting micro zonation of earthquakes with microtremor analysis in the Tirtoyudo sub-district, Malang Regency stated that several villages were significantly affected by the earthquake had low natural frequency (f_0) values ranging from 1.28 – 13.23 Hz, the value Soil amplification (A_0) ranged from 1.33 – 10.77, seismic vulnerability index values (Kg) ranged from 0.13 – 29.91 [40]. Some of these villages include Wirotaman Village and Sonowangi Village. In this case, the same result was found that Wirotaman Village at point SA 05 is known to have a low dominant frequency (f_0) value (<2.5 Hz), and there is also a known indication of a fault; this is supported by the results of geoelectrical resistivity analysis showing a low resistivity value (62.2 Ω) which is suspected to be a type of clay.

The advantages of this research based on the geoelectrical resistivity survey can be shown in the subsurface cross-section of the area where there is an indication of a fault; this is supported by the low value of the dominant soil frequency (f_0) at that point. The results of this study can be continued by adding several other parameters, such as thickness, the value of shear wave velocity (vs), the value of Vs30, PGA, and drilling data in the area.

4. Conclusion

The results of this study show the correlation between the results of the HVSR curve analysis and geoelectrical resistivity in determining the seismic vulnerability of an area. Further analysis of areas with a high seismic vulnerability index using the geoelectrical resistivity method shows that seismically vulnerable areas are associated with low resistivity values. The layer with low resistivity values intrudes into the layer with high resistivity to the surface, marked by the appearance of several springs. This is identified as the presence of new faults. This study demonstrates a correlation between the extent of building damage caused by the April 10, 2021 earthquake and the results of the HVSR curve analysis. The places with the most severe damage have a high seismic vulnerability index (K_g=12-18). This suggests a relatively dense sediment deposit. These locations are scattered between points SA 05 and SA 06, southwest of the study site. This region is the most vulnerable to earthquake-related damage. In addition, based on information obtained from the field, point SA 05 is the location with the most severe level of damage.

The resistivity values derived from 2D geoelectric resistivity modeling with a dipole-dipole configuration reveal the distribution of clay (1.99-7.89 Ωm) on the surface, sandy loam (7.90-62.1 Ωm) and breccias (62.2- 246 Ωm) as bedrock. The existence of a lithology layer with a low resistivity value is interpreted as a clay layer; this layer indicates the presence of a weak zone which is associated with the presence of fractures. Several points of damage at the SA 05 location are on one line; this condition is associated with the possibility of new faults. The emergence of new faults may occur, considering that the location of SA 05 is quite close to the fault that separates the Wuni and Mandalika formations. Consequently, the findings of this study demonstrate that microtremor and geoelectrical resistivity surveys can accurately depict a region's seismic hazard and underlying characteristics, both the thickness of the sediment and the presence of subsurface structures, particularly faults, in an area. In this case, minor faults at the study site are found with a Southeast-Southwest orientation through the interpretation of subsurface resistivity data. However, this research is still preliminary; further research to determine the subsurface structure can be carried out through correlation analysis of HVSR data and subsurface resistivity with drilling data.

5. Declarations

5.1. Author Contributions

Conceptualization, A.S. and A.M.J.; methodology, A.S. and F.A.; software, F.H. and S.R.; validation, A.S., A.M.J., and M.F.R.H.; formal analysis, A.S., F.H., S.R., and M.F.R.H.; investigation, F.R. and S.R.; resources, A.S. and F.A; data curation, A.S., A.M.J., and F.A.; writing—original draft preparation, A.S., F.H., and S.R.; writing—review and editing, A.M.J., F.A., and M.F.R.H.; visualization, F.H. and M.F.R.H.; supervision, A.S.; project administration, F.A., and F.H. All authors have read and agreed to the published version of the manuscript.

5.2. Data Availability Statement

The data presented in this study are available on request from the corresponding author.

5.3. Funding and Acknowledgements

The authors would like to express their gratitude to FMIPA Universitas Brawijaya for their financial support through Hibah Guru Besar FMIPA 2022 with grant number 3084.15/UN10.F09/PN/2022, in which the first author serves as the principal researcher.

5.4. Conflicts of Interest

The authors declare no conflict of interest.

6. References

[1] BPBD Malang Regency. (2022). Data on Disaster Events in Malang Regency. Regional Disaster Management Agency of Malang District, Malang Regency Government, Malang, Indonesia.

[2] BMKG. (2021). Recent Earthquakes (M ≥ 5.0). Government of Indonesia: Meteorology, Climatology, and Geophysical Agency. Badan Meteorologi, Klimatologi, dan Geofisika, Jakarta, Indonesia. Available online: https://www.bmkg.go.id/gempabumi-terkini.html (accessed on April 2023). (In Indonesian)

[3] Kanai, K. (1983). Engineering seismology. University of Tokyo Press, Tokyo, Japan.

[4] Nakamura, Y. (1989). Method for dynamic characteristics estimation of subsurface using microtremor on the ground surface. Quarterly Report of RTRI (Railway Technical Research Institute) (Japan), 30(1), 25–33.

[5] Akkaya, İ. (2020). Availability of seismic vulnerability index (K g) in the assessment of building damage in Van, Eastern Turkey. Earthquake Engineering and Engineering Vibration, 19(1), 189–204. doi:10.1007/s11803-020-0556-z.

[6] Lermo, J., & Chávez-García, F. J. (1994). Site effect evaluation at Mexico City: Dominant period and relative amplification from strong motion and microtremor records. Soil Dynamics and Earthquake Engineering, 13(6), 413–423. doi:10.1016/0267-7261(94)90012-4.

[7] Mahajan, A. K., Mundepi, A. K., Chauhan, N., Jasrotia, A. S., Rai, N., & Gachhayat, T. K. (2012). Active seismic and passive microtremor HVSR for assessing site effects in Jammu city, NW Himalaya, India-A case study. Journal of Applied Geophysics, 77, 51–62. doi:10.1016/j.jappgeo.2011.11.005.

[8] Putti, S. P., & Satyam, N. (2020). Evaluation of Site Effects Using HVSR Microtremor Measurements in Vishakhapatnam (India). Earth Systems and Environment, 4(2), 439–454. doi:10.1007/s41748-020-00158-6.

[9] Haerudin, N., Rustadi, Alami, F., & Yogi, I. B. S. (2020). The effect site analysis based on microtremor data using the Horizontal to Vertical Spectral Ratio (HVSR) method in the Bandar Lampung City. Journal of Physics: Conference Series, 1572(1), 012075. doi:10.1088/1742-6596/1572/1/012075.

[10] Widia Pamungkas Isburhan, R., Nuraeni, G., Verdhora Ry, R., Yudistira, T., Cipta, A., & Cummins, P. (2019). Horizontal-to-Vertical Spectral Ratio (HVSR) Method for Earthquake Risk Determination of Jakarta City with Microtremor Data. IOP Conference Series: Earth and Environmental Science, 318(1), 12033. doi:10.1088/1755-1315/318/1/012033.

[11] Stanko, D., Markušić, S., Gazdek, M., Sanković, V., Slukan, I., & Ivančić, I. (2019). Assessment of the seismic site amplification in the city of ivanec (NW part of Croatia) using the microtremor HVSR method and equivalent-linear site response analysis. Geosciences (Switzerland), 9(7), 312. doi:10.3390/geosciences9070312.

[12] Fat-Helbary, R. E. S., El-Faragawy, K. O., & Hamed, A. (2019). Application of HVSR technique in the site effects estimation at the south of Marsa Alam city, Egypt. Journal of African Earth Sciences, 154, 89–100. doi:10.1016/j.jafrearsci.2019.03.015.

[13] Yaghmaei-Sabegh, S., & Rupakhety, R. (2020). A new method of seismic site classification using HVSR curves: A case study of the 12 November 2017 Mw 7.3 Ezgeleh earthquake in Iran. Engineering Geology, 270, 105574. doi:10.1016/j.enggeo.2020.105574.

[14] Theodoulidis, N., Dushi, E., Duni, L., Grendas, I., Panou, A., Hajrullai, A., Kuka, N., & Koci, R. (2022). Local Site Effects Investigation in Durres City (Albania) Using Ambient Noise, after the 26 November 2019 (M6.4) Destructive Earthquake. Applied Sciences (Switzerland), 12(22), 11309. doi:10.3390/app122211309.

[15] Li, J., Zhou, B., Rong, M., Chen, S., & Zhou, Y. (2020). Estimation of source spectra, attenuation, and site responses from strong-motion data recorded in the 2019 Changning earthquake sequence. Bulletin of the Seismological Society of America, 110(2), 410–426. doi:10.1785/0120190207.

[16] Cetin, K. O., Altun, S., Askan, A., Akgün, M., Sezer, A., Kıncal, C., Özdağ, Ö. C., İpek, Y., Unutmaz, B., Gülerce, Z., Özacar, A. A., Ilgaç, M., Can, G., Cakir, E., Söylemez, B., El-Sayeed, A., Zarzour, M., Bozyiğit, İ., Tuna, Ç., … Karaali, E. (2022). The site effects in Izmir Bay of October 30 2020, M7.0 Samos Earthquake. Soil Dynamics and Earthquake Engineering, 152, 107051. doi:10.1016/j.soildyn.2021.107051.

[17] Reynolds, J. M. (2011). An introduction to applied and environmental geophysics. John Wiley & Sons, Hoboken, United States.

[18] Robot, L. C., Manyoe, I. N., Arifin, Y. I., Saputra, M. J. A., Bilgais, A. A., Abdullah, R. A., & Napu, S. S. S. (2021). Surface and subsurface analysis based on the geological structure and electrical resistivity Data in Gorontalo Outer Ring Road (GORR), Huidu Utara. Journal of Physics: Conference Series, 1968(1), 12054. doi:10.1088/1742-6596/1968/1/012054.

[19] Susilo, A., Fitriah, F., Sunaryo, Ayu Rachmawati, E. T., & Suryo, E. A. (2020). Analysis of landslide area of Tulung subdistrict, Ponorogo, Indonesia in 2017 using resistivity method. Smart and Sustainable Built Environment, 9(4), 341–360. doi:10.1108/SASBE-06-2019-0082.

[20] Hossain, M. B., Roknuzzaman, M., & Rahman, M. M. (2022). Liquefaction Potential Evaluation by Deterministic and Probabilistic Approaches. Civil Engineering Journal, 8(7), 1459-1481. doi:10.28991/CEJ-2022-08-07-010.

[21] Hasan, M. F. R., Salimah, A., Susilo, A., Rahmat, A., Nurtanto, M., & Martina, N. (2022). Identification of Landslide Area Using Geoelectrical Resistivity Method as Disaster Mitigation Strategy. International Journal on Advanced Science, Engineering and Information Technology, 12(4), 1484–1490. doi:10.18517/ijaseit.12.4.14694.

[22] Chasanah, U., Handoyo, E., Rahmawati, N. N., & Musfiana, M. (2022). Mapping Risk Level Based on Peak Ground Acceleration (PGA) and Earthquake Intensity Using Multievent Earthquake Data in Malang Regency, East Java, Indonesia. Journal of Physical Science, 14(1), 64–72. doi:10.25077/jif.14.1.64-72.2022.

[23] Muntafi, Y., & Nojima, N. (2021). The Spatio-temporal Tectonic Condition and Microzonation Map of Malang Region after the 2021 M6.1 Malang Earthquake for Disaster Risk Mitigation. IOP Conference Series: Earth and Environmental Science, 933(1), 12031. doi:10.1088/1755-1315/933/1/012031.

[24] Tawakal, M. I., Haris, A., & Martha, A. A. (2020). Estimating shear wave velocity (Vs30) of East Java, Indonesia, using ambient noise inversion of horizontal to vertical spectral ratio (HVSR). IOP Conference Series: Earth and Environmental Science, 538(1), 12012. doi:10.1088/1755-1315/538/1/012012.

[25] Keskinsezer, A., & Dağ, E. (2019). Investigating of soil features and landslide risk in Western-Atakent (İstanbul) using resistivity, MASW, Microtremor and boreholes methods. Open Geosciences, 11(1), 1112–1128. doi:10.1515/geo-2019-0086.

[26] Khalili, M., & Mirzakurdeh, A. V. (2019). Fault detection using microtremor data (HVSR-based approach) and electrical resistivity survey. Journal of Rock Mechanics and Geotechnical Engineering, 11(2), 400–408. doi:10.1016/j.jrmge.2018.12.003.

[27] Demirci, A., Kaya, M. A., Bekler, T., & Ekinci, Y. L. (2007). Microtremor and Resistivity Studies for Evaluating Ground Conditions in Canakkale. Near Surface 2007 - 13th EAGE European Meeting of Environmental and Engineering Geophysics. doi:10.3997/2214-4609.20146621.

[28] Zhu, C., Pilz, M., & Cotton, F. (2020). Evaluation of a novel application of earthquake HVSR in site-specific amplification estimation. Soil Dynamics and Earthquake Engineering, 139, 106301. doi:10.1016/j.soildyn.2020.106301.

[29] Talha Qadri, S. M., Nawaz, B., Sajjad, S. H., & Sheikh, R. A. (2015). Ambient noise H/V spectral ratio in site effects estimation in Fateh Jang area, Pakistan. Earthquake Science, 28(1), 87–95. doi:10.1007/s11589-014-0105-9.

[30] Bour, M., Fouissac, D., Dominique, P., & Martin, C. (1998). On the use of microtremor recordings in seismic microzonation. Soil Dynamics and Earthquake Engineering, 17(7–8), 465–474. doi:10.1016/S0267-7261(98)00014-1.

[31] Telford, W. M., Geldart, L. P., & Sheriff, R. E. (1990). Applied geophysics. Cambridge University Press, 792. doi:10.1017/CBO9781139167932.

[32] van Bemmelen, R.W. (1949). General Geology of Indonesia and Adjacent Archipelagoes. Government Printing Office, The Hague, Netherlands.

[33] Sujanto, R., Hadisantono, R., Chaniago, R., & Baharuddin, R. (1992). Geological Map of The Turen Quadrangle, Jawa. Geological Research and Development Centre, Bandung, Indonesia.

[34] Khan, S., Waseem, M., & Jan, S. (2021). Site response studies in Peshawar using the Nakamura technique of HVSR. Arabian Journal of Geosciences, 14(3). doi:10.1007/s12517-021-06527-3.

[35] Meunier, P., Hovius, N., & Haines, J. A. (2008). Topographic site effects and the location of earthquake induced landslides. Earth and Planetary Science Letters, 275(3–4), 221–232. doi:10.1016/j.epsl.2008.07.020.

[36] Kramer, S. L. (1996). Geotechnical earthquake engineering. Pearson Education India, Noida, India.

[37] Nakamura, Y. (2000). Clear identification of fundamental idea of Nakamura's technique and its applications. Proceedings of the 12th world conference on earthquake engineering, 30 January-4 February, Auckland, New Zealand.

[38] Khalqillah, A., Muksin, U., Musfirah, Ningsih, W. A., & Irwandi. (2019). SVIM: A Program for Seismic Vulnerability Index Determination and HVSR Data Processing. IOP Conference Series: Earth and Environmental Science, 273(1), 012016. doi:10.1088/1755-1315/273/1/012016.

[39] Prabowo, U. N., Amalia, A. F., & Wiranata, F. E. (2018). Local site effect of soil slope based on microtremor measurement in Samigaluh, Kulon Progo Yogyakarta. Journal of Physics: Conference Series, 997(1), 12007. doi:10.1088/1742-6596/997/1/012007.

[40] Rochman, J. P. G. N., Sadewa, M. A., & Putra, A. M. (2023). Earthquake Microzonation Using Microtremor Analysis and Horizontal to Vertical Spectral Ratio Method Study Case at Ampelgading and Tirtoyudo Sub-district, Malang, East Java. Advances in Engineering Research, 127–136. doi:10.2991/978-94-6463-148-7_14.